Agricultural Water Management 98 (2011) 606–618

Contents lists available at ScienceDirect

Agricultural Water Management

journal homepage: www.elsevier.com/locate/agwat

# Enhancing the Simplified Surface Energy Balance (SSEB) approach for estimating landscape ET: Validation with the METRIC model

G.B. Senay*, M.E. Budde[1], J.P. Verdin[2]

*U.S. Geological Survey (USGS), Earth Resources Observation and Science (EROS) Center, 47914 252nd St, Sioux Falls, SD 57198, United States*

ARTICLE INFO

*Article history:*
Received 5 March 2010
Accepted 23 October 2010
Available online 30 November 2010

*Keywords:*
Evapotranspiration
Energy balance
Surface temperature
NDVI
METRIC

ABSTRACT

Evapotranspiration (ET) can be derived from satellite data using surface energy balance principles. METRIC (Mapping EvapoTranspiration at high Resolution with Internalized Calibration) is one of the most widely used models available in the literature to estimate ET from satellite imagery. The Simplified Surface Energy Balance (SSEB) model is much easier and less expensive to implement. The main purpose of this research was to present an enhanced version of the Simplified Surface Energy Balance (SSEB) model and to evaluate its performance using the established METRIC model. In this study, SSEB and METRIC ET fractions were compared using 7 Landsat images acquired for south central Idaho during the 2003 growing season. The enhanced SSEB model compared well with the METRIC model output exhibiting an $r^2$ improvement from 0.83 to 0.90 in less complex topography (elevation less than 2000 m) and with an improvement of $r^2$ from 0.27 to 0.38 in more complex (mountain) areas with elevation greater than 2000 m. Independent evaluation showed that both models exhibited higher variation in complex topographic regions, although more with SSEB than with METRIC. The higher ET fraction variation in the complex mountainous regions highlighted the difficulty of capturing the radiation and heat transfer physics on steep slopes having variable aspect with the simple index model, and the need to conduct more research. However, the temporal consistency of the results suggests that the SSEB model can be used on a wide range of elevation (more successfully up 2000 m) to detect anomalies in space and time for water resources management and monitoring such as for drought early warning systems in data scarce regions. SSEB has a potential for operational agro-hydrologic applications to estimate ET with inputs of surface temperature, NDVI, DEM and reference ET.

Published by Elsevier B.V.

## 1. Introduction

Evapotranspiration (ET) is an important and primary component of the hydrologic budget because it expresses the exchange of mass and energy between the soil–water–vegetation system and the atmosphere. Prevailing weather conditions influence potential and reference ET through forcing variables such as radiation, temperature, wind, and relative humidity. In addition to these weather variables, actual ET (ETa) is also affected by land cover type and condition and soil moisture. ETa's dependence on land cover and soil moisture, and its direct relationship with carbon dioxide assimilation in plants, makes it an important variable to monitor and estimate crop yield and biomass for decision makers interested in food security, grain markets, water allocation and carbon sequestration (Bastiaanssen et al., 2005).

Surface energy balance methods for ET estimation have been successfully applied by several researchers (Jackson et al., 1981; Moran et al., 1996; Bastiaanssen et al., 1998, 2005; Kustas and Norman, 2000; Roerink et al., 2000; Allen et al., 2005, 2007a,b; Su, 2002; Su et al., 2005; Anderson et al., 1997, 2007) to estimate agricultural crop water use and ET by general landscapes. A comprehensive summary of the various surface energy balance models is presented by Gowda et al. (2008) and Kalma et al. (2008). The approach of most energy balance models requires solving the energy balance (Eq. (1)) at the land surface, where the latent heat flux, comparable to ETa, is calculated as the residual of the difference between the net radiation to the surface and losses due to the sensible heat flux

*Abbreviations:* $\alpha$, correction coefficient to convert grass reference ET to alfalfa (maximum) reference; ET, it can be assumed or developed using local calibration; DEM, elevation data from a digital elevation model; ETf, reference (maximum) ET fraction from the SSEB model; ETo, standardized clipped grass reference ET; ETm, maximum ET ($\alpha$ETo); ETrF, reference (alfalfa) ET fraction from the METRIC model; $K_L$, lapse rate correction; LST, land surface temperature; LSTc, elevation corrected LST; METRIC, Mapping EvapoTranspiration at high Resolution with Internalized Calibration; NDVI, normalized difference vegetation index; SSEB, Simplified Surface Energy Balance model; SSEBel, SSEB with elevation correction alone; SSEBelvi, SSEB with both elevation and NDVI correction; Ta, air temperature (weather data); Ts, land surface temperature (as observed by remotely sensed data).

* Corresponding author. Tel.: +1 605 594 2758; fax: +1 605 594 6529.
*E-mail addresses:* senay@usgs.gov (G.B. Senay), mbudde@usgs.gov (M.E. Budde), verdin@usgs.gov (J.P. Verdin).
[1] Tel.: +1 605 594 2619.
[2] Tel.: +1 303 497 6930.

0378-3774/$ – see front matter. Published by Elsevier B.V.
doi:10.1016/j.agwat.2010.10.014

**Table 1**
Comparison between SSEB and METRIC parameters and calculation procedures.

| Parameter | SSEB | METRIC |
|---|---|---|
| ETa | ETf × ETm | ETrF × ETr_24 |
| ET fraction | ETf = (TH − *Tx*)/(TH − TC)<br>Adjusted for elevation and cover fraction using NDVI and DEM | ETrF = ETinst/ETr |
| ETinst | NA | Rn − *H* − *G* |
| Rn (net radiation) | Included as part of ETo for a reference crop f(incoming shortwave, reference crop albedo, wind, RH, temperature, pressure) | f(solar constant, albedo, LST and NDVI) |
| *H* (sensible heat flux) | NA | $(\rho \cdot Cp \cdot dT)/r_{ah}$ |
| *G* (ground heat flux) | NA | Rn/*G* = f(NDVI, LST) |
| Advantage | Simple to implement on a global scale | Process understanding: solves all energy balance terms |
| Limitation | Does not solve for sensible and ground heat fluxes | More time and cost intensive |

*Note*: ETinst = instantaneous ET at the time of satellite overpass, $\rho$ = air density in kg/m$^3$, Cp = air specific heat (J/kg/K), $r_{ah}$ = aerodynamic heat resistance to heat transport, dT = temperature difference between surface and air, ETm = maximum ET, $\alpha \times$ ETo (grass reference ET), ETf = ET fraction, ETr = hourly alfalfa reference ET, ETr_24 = 24 h alfalfa reference ET.

(energy used to heat the air) and ground heat flux (energy stored in the surface).

The surface energy balance is of the form:

$$LE = Rn - G - H \quad (1)$$

where LE = latent heat flux (energy consumed by evapotranspiration) (W/m$^2$); Rn = net radiation at the surface (W/m$^2$); *G* = ground heat flux (W/m$^2$); *H* = sensible heat flux (W/m$^2$).

Research has shown that spectral vegetation index (*SVI*) and surface temperature (*Ts*) observations from satellite sensors such as AVHRR (Advanced Very High Resolution Radiometer), MODIS (Moderate Resolution Imaging Spectroradiometer), Landsat and ASTER (Advanced Spaceborne Thermal Emission and Reflection Radiometer) are useful for quantifying the energy absorption and exchange processes (Moran et al., 1996; Goward et al., 1994; Choudhry, 1991; Nemani et al., 1993). Satellite derived land surface temperatures have been shown to be a function of energy exchange processes that are controlled by the sources of net radiation (soil vs. vegetation) and water availability for evapotranspiration (Goward et al., 1985; Moran et al., 1989; Price, 1989; Nemani et al., 1993). Lower surface temperatures generally mean higher evapotranspiration due to either higher canopy density or high surface moisture content (Nemani and Running, 1989; Choudhry, 1991; Nemani et al., 1993; Goward et al., 1994; Moran et al., 1996; Bastiaanssen et al., 1998, 2005).

The Simplified Surface Energy Balance, SSEB (Senay et al., 2007) approach was developed as a simplified procedure to provide rapid estimates of ET over large areas where high accuracy, Allen et al. (2007a), afforded by the more labor intensive, more complex energy balance models such as METRIC (Mapping EvapoTranspiration at high Resolution with Internalized Calibration) is not cost effective. The enhancement to the existing SSEB model includes correction for land surface elevation and land cover condition. A summary comparison between SSEB and METRIC in terms of data requirements and key-parameter estimation is presented in Table 1.

## 2. Background

Although solving the full energy-balance approach has been shown to give good results, the data and skill requirements to solve the various terms in the equation can be challenging for operational applications in large, data-sparse regions. For example, most SEBAL applications require measurement of wind speed and relatively intense, iterative calibration, determination and review by an experienced operator. METRIC, a derivative of SEBAL, uses reference ET for calibration and requires relatively high quality weather data sets that include solar radiation, air temperature, humidity and wind speed, preferably on an hourly or shorter basis (Allen et al., 2007a). However, Allen (2010, Pers. Comm.) show that METRIC's ETrF (reference ET fraction) is relatively insensitive to the accuracy of hourly ETr (reference ET) used to calibrate the surface energy balance. Processing costs for applying models such as SEBAL and METRIC may run as high as $1000–5000 per image and $20,000–80,000 per year (for seasonal ET estimation) per typical Landsat scene-sized area (160 km × 160 km) (Allen, 2010, Pers. Comm.). The relatively high costs are for human oversight and quality control of the calibration of the full energy balance process. As an alternative, the SSEB approach of Senay et al. (2007), may be suitable for operational applications to estimate ET at a large scale for basin wide water budget analysis where highly accurate estimates of ET are not required.

The SSEB works similar to the more complex surface energy balance models in that *Ts* is used as a primary scalar. However, whereas in the complex models, the temperature scalar is applied in an aerodynamic estimation of sensible heat flux (*H*) that is in turn subtracted from estimates of net radiation and soil heat flux to determine ET, the SSEB temperature scalar is multiplied directly by the estimate of maximum ET. Moran et al. (1994, 1996) formulated a similar approach that developed a ratio of actual ET to potential ET using the "trapezoid" approach in a Vegetation Index (VI) vs. (Ts − Ta) (surface temperature minus air temperature) space to determine field water deficit for partially vegetated surfaces. The link between maximum ET as formulated by Penman–Monteith and land surface temperature was initially made by Jackson et al. (1981) in the development of the Crop Water Satisfaction Index (CWSI) for plant stress detection. While there are similarities in the general concept between SSEB and CWSI or the trapezoid method, the CWSI requirement for foliage temperature prohibits its use in partially vegetated surfaces (Moran et al., 1994). Furthermore, the SSEB method has an advantage over the trapezoid in that it does not require the use of air temperature and knowledge of land cover types to calculate the ET fraction. The SSEB uses the principle of the "hot" and "cold" pixel approach of Bastiaanssen et al. (1998) and Allen et al. (2007a) that provides the basis to convert LST into an ET fraction without the need for air temperature. The operational simplicity of the SSEB method in comparison with the trapezoid or SEBAL/METRIC can be attributed to the absence of an air temperature (as required by trapezoid method) and agronomic parameter requirements for surface roughness and aerodynamic resistance parameters. Particularly, the avoidance of using the air temperature (Ta) measured from a meteorological station in combination with LST measured by a satellite sensor in absolute magnitude is very important. The two data sets (LST and Ta) may not be comparable in absolute sense; for example, Moran et al. (1996) reported that Landsat-based LST was consistently higher than ground based-LST by as much as 3 °C which could cause an error of 50 W/m$^2$ in the estimation of ET for every 1 °C error in LST. With a 2.45 MJ/kg latent heat of vaporization for water, 50 W/m$^2$ latent heat energy is equivalent to 1.76 mm ET. For more detailed understanding of the

complex relationships between vegetation cover, land surface temperature, energy balance and ET, readers are advised to refer to the pioneering research works such as Moran et al. (1994), Bastiaanssen et al. (1998) and Allen et al. (2005, 2007a).

The SSEB approach estimates ETa using the relative ET fractions scaled from thermal imagery in combination with a spatially explicit maximum reference ET. In the original SSEB formulation, differences in surface temperature across homogeneous terrain are assumed to be primarily associated with differences in vegetation and soil water consumption rates. The consequence is that impacts of albedo and soil heat flux on total available energy are ignored. This can cause an underestimate of ET for low albedo surfaces and overestimate of ET for high albedo surfaces, and similarly an overestimate of ET for surfaces having high soil heat flux densities, such as for most bare soils. We believe the proposed enhancements will improve these shortcomings especially on an agricultural and naturally vegetated environment where the albedo values remain in a close range, less than 0.3. Roerink et al. (2000) reported that land surface temperature as a function of albedo stabilizes between the ranges of 0.2 and 0.28.

### 2.1. Model enhancement justification

The most significant topographic factors in determining land surface temperature (LST), given similar conditions of surface wetness, have been found empirically to be elevation, slope and aspect (relative to solar illumination) (Florinsky et al., 1994). In high elevation areas, the land surface temperature can be affected by both elevation and aspect which make it risky to solely rely on the lapse rate correction. Furthermore, the assumption of a linear relationship between LST and ET can be challenged when the albedo and ground-heat flux characteristics of a landscape (pixel) differ markedly from a green vegetation–soil complex of a reference crop. This is well summarized by Warner and Chen (2001) who stated that the temperature of an object on the surface of the Earth is dependent on the summation of radiative, convective, conductive and latent heat transfer between the object and its surroundings over the diurnal period.

Dexter (1999) reported that the albedo of a wheat field varies during the season with a steady increase from around 0.1 during planting, depending on soil characteristics, to a plateau of 0.17 during mature vegetation with a further increase during senescence to 0.22 at harvest. The additional increase in albedo during senescence by 0.05 constitutes a 29% increase from the green vegetation. This will reduce the net radiation, potentially giving rise to a cooler surface temperature for the same wetness condition that may not be directly attributed to ET in comparison to bare soil. On the other hand, when senescence reduces the stomatal conductance of the vegetation, ET can be expected to decrease and LST to rise in comparison to a green vegetation. Several researchers (Menenti and Choudhury, 1993; Bastiaanssen et al., 1998; Roerink et al., 2000) have presented a functional relationship between surface albedo, surface temperature and evaporative fraction.

Although the SSEB model, driven by the ET fraction calculated from the thermal data, seems to provide reasonable ET estimation for irrigated fields with uniform topography, we propose a simple modification that uses readily available Normalized Difference Vegetation Index (NDVI) data to account for differences in soil–vegetation complex in relation to a reference crop environment. As stated earlier, one of the weaknesses of the SSEB model is its lack of land cover specific albedo-based parameterization. The ETa derived from the SSEB model is in reference to a clipped grass reference ET with an albedo of 0.23 which is included in the ETo formulation. In addition to albedo, SSEB does not calculate ground and sensible heat fluxes. The calculation of the two flux terms uses NDVI with the complex energy balance models such as METRIC and SEBAL in parameterization of the aerodynamic resistance ($r_{ah}$) (Allen et al., 2007a). Thus, in order to improve the robustness of the SSEB model so that it can be applied in diverse vegetation and topographic conditions, we propose a simple NDVI-based correction.

The main objectives of this study were: (1) to present an enhancement to the SSEB model that improves its application to complex topography (having varying slope and aspect) and to land cover mixtures having different proportions of green, bare and senesced vegetation and (2) to present a comparison of the SSEB model output with the METRIC model.

Two types of model enhancements were applied to SSEB. The first one was the use of a DEM-based lapse-rate correction factor to account for land surface temperature differences caused by topography alone. Secondly, the NDVI was used to correct differences between the SSEB and METRIC models that seem to relate to the amount of vegetation cover (or lack of).

## 3. Methods

### 3.1. Data

The most important data sets used in this study are seven Landsat-based thermal and short-wave reflectance images acquired over south central Idaho from April through August, 2003. In addition, a 1-km digital elevation model data set from Hydro1K (Verdin and Jenson, 1996) was used to correct the effect of elevation on land surface temperature. Other data sets included model outputs of ETrF from the METRIC process produced by Allen et al. (2004) and Tasumi et al. (2005) and reference ET calculated from global weather data sets (Senay et al., 2008).

The seven Landsat image dates are shown in Table 2. All images except 5/19/2003 (Landsat 7) are from Landsat 5. All Landsat images were processed by the University of Idaho as part of the METRIC ET modeling exercise (Allen et al., 2007b, 2004). METRIC ETrF (reference ET fraction) grids were made available to the USGS/EROS group for comparison with the SSEB model output. NDVI grids were calculated at EROS from the provided images. The SSEB modeling approach was used to derive two sets of SSEB ET fractions using the Landsat thermal and NDVI data sets. More details of the SSEB ETf will be discussed in the following sections.

METRIC-derived ETrF was obtained from the University of Idaho for the 7 image dates at 30 m spatial resolution. The ETrF parameter is synonymous with the well-known crop coefficient (Kc) and, in the case of METRIC, ETrF is based on the alfalfa reference ETr. Values for ETr are commonly about 1.2–1.3 times grass reference ETo due to the taller, rougher and leafier characteristics of alfalfa. Although the thermal data set for Landsat 5 is 120 m and 90 m for Landsat 7, METRIC calculated ETrF values at 30 m resolution matching the resolution of the Landsat 5 NDVI data set. Accordingly, SSEB model outputs were also generated at 30 m resolution.

As part of an operational global product, daily grass reference ETo generated using standardized Penman–Monteith equation (Allen et al., 1998, 2006) from global weather fields of the Global Data Assimilation System (GDAS) as described in Senay et al. (2008), was used to estimate ETa in conjunction with ETf or ETrF. The calculation of SSEB ETf is not tied to a specific reference crop as in METRIC's ETrF (alfalfa), but it can be considered as the fraction of the maximum ET or ETm (Eq. (4)).

Thermal digital numbers (DNs) of Landsat data were converted to land surface temperature (LST) in Kelvin using standard calibration equations and coefficients as shown in Markham and Barker (1986) in a two-step procedure: (1) convert the DNs to radiance values using the bias and gain coefficients specific to the sensor and (2) convert the radiance data to Kelvin. Since the thermal data were used in a relative sense for each imagery, i.e., recalibrated

**Table 2**
Daily and seasonal values of ET fractions, ETm and ETa for a representative sampling point (ID20, shown in Fig. 3b).

| Image date | ETrF METRIC | ETf SSEBelvi | NDVI | ETm (mm) | ETa METRIC (mm) | ETa SSEBelvi (mm) |
|---|---|---|---|---|---|---|
| 04/09/03 | 0.37 | 0.20 | 0.00 | 4.08 | 1.51 | 0.82 |
| 05/19/03 | 0.02 | 0.16 | 0.00 | 6.00 | 0.12 | 0.96 |
| 05/27/03 | 0.04 | 0.05 | 0.01 | 7.27 | 0.29 | 0.36 |
| 06/28/03 | 0.81 | 0.76 | 0.46 | 9.37 | 7.59 | 7.12 |
| 07/14/03 | 0.93 | 0.99 | 0.72 | 8.32 | 7.73 | 8.23 |
| 07/30/03 | 0.93 | 0.98 | 0.76 | 8.12 | 7.56 | 8.23 |
| 08/31/03 | 0.83 | 0.86 | 0.66 | 5.28 | 4.38 | 4.54 |
| Seasonal[a] daily average | 0.55 | 0.56 | 0.36 | 7.0 | 4.14 | 4.26 |
| Seasonal sum | | | | 1008 | 596 | 613 |

[a] Period-weighted values were used to obtain seasonal averages. The seasonal period consists of 144 days between April 9 and August 31, 2003.
*Note*: NDVI = 0.0 is a result of using digital numbers instead of reflectance values for NDVI calculations.

between the hot and cold pixels with in the image, we did not conduct atmospheric correction which is recommended for multi-date processing of imagery.

### 3.2. SSEB model overview and parameter estimation

The main concept of the SSEB approach in Senay et al. (2007) is the joint use of reference ET and land surface temperature data. The surface energy balance is first solved for a reference crop condition (assuming full vegetation cover and unlimited water supply) using the standardized Penman–Monteith equation (Allen et al., 1998). A global application of the P–M equation is documented in Senay et al. (2008). ET fractions (ETf) account for differences in water availability in the landscape; and are used to adjust the reference ET (ETo) based on the LST of the pixel (Eq. (2) for ETf).

In the SSEB model formulation, ET fractions are calculated from the LST data sets based on the assumptions that *hot* pixels experience little or no ET (Bastiaanssen et al., 1998; Allen et al., 2005), *cold* pixels represent "maximum" ET, and, with the simplified assumption, that ET can be scaled between these values in proportion to LST. Allen et al. (2005, 2007a) have outlined a procedure for using a water balance approach to determine the ET of a moist bare soil in case satellite images are acquired after rainfall events. This ET estimate is used to define the ET fraction for the hot pixel.

In principle, instantaneous LST at satellite overpass time can be used to identify *hot* and *cold* pixels which in turn can be used to calculate proportional fractions of ET on a per pixel basis. The *hot* and *cold* pixels are selected using an NDVI image as a guide to identify dry and bare areas for the *hot pixels.* Similarly, the *cold* pixels are selected from well-watered, well-vegetated areas or nearby water bodies.

In this study, irrigated areas were used to select the cold pixels (Fig. 1), following similar procedures used in METRIC (Allen et al., 2007a). Cool (lower LST) center pivot irrigation fields with NDVI > 0.4 (April 9, 2003) and NDVI > 0.70 for the rest of the season were used for guidance. The hot pixels were selected from bare areas (NDVI < 0.2) found close to irrigated fields based on the guidance and justification provided by Allen et al. (2007a) to avoid desert soil pixels that may develop crusts and delamination with mulches which in turn tend to reduce the thermal conductivity of the surface that again reduces soil heat flux density. Choosing desert pixels for the "hot" would result in unrealistically higher ET values for the generally cooler (which maybe be wrongly attributed to ET) but dry bare agricultural soils due to their relatively higher ground heat conductivity.

The ET fraction (ETf) is calculated for each pixel "*x*" by applying Eq. (2) to each of the 7-date Landsat LST grids.

$$\mathrm{ETf} = \frac{\mathrm{TH} - Tx}{\mathrm{TH} - \mathrm{TC}} \quad (2)$$

where TH is the average of the representative 3 *hot* pixels selected for hot "bare" areas.; TC is the average of representative 3 *cold* pixels selected from the irrigated fields; and *Tx* is the LST value for any given pixel in the image.

The basic approach of calculating ETa involves only two steps: ETa is simply a product of the ET fraction (ETf) and ETo via Eqs. (3) and (4).

$$\mathrm{ETa} = \mathrm{ETf} \times \mathrm{ETm} \quad (3)$$

where ETa is actual ET, ETf is ET fraction, and ETm is maximum ET for the region. When grass reference ETo is calculated from weather data, ETm is estimated as:

$$\mathrm{ETm} = \alpha \times \mathrm{ETo} \quad (4)$$

where the multiplier $\alpha$ is recommended to be 1.2 to estimate ET for tall, full cover crops such as alfalfa, corn and wheat.

Crops such as alfalfa, corn and wheat are aerodynamically rougher than the clipped grass reference and have greater leaf area and thus greater canopy conductance (Allen et al., 1998). Thus, the 1.2 multiplier is not needed if ETr (based on alfalfa crop) is used instead of ETo. Alternatively, $\alpha$ can be determined using localized calibration such as one with Gowda et al. (2009) who determined $\alpha$ to be 1.1 using Lysimeter data in the Texas Panhandle.

### 3.3. Model enhancements

The following enhancements have been made to SSEB to improve its accuracy over a wider range of terrain and land cover conditions.

#### 3.3.1. Elevation

Although the SSEB was developed mainly to monitor relatively homogeneous irrigation fields over flat topography, simple corrections such as the DEM-based lapse-rate were applied to permit application of SSEB to more complex landscapes having variable elevation. So far the only major comparisons of the SSEB algorithm were conducted by Gowda et al. (2009) where they found strong correlation ($r^2 = 0.84$) against Lysimeter data on homogeneous terrain. In the improved model, Eq. (5) was used to account for LST differences caused by elevation differences. This is a similar formulation as reported in Allen et al. (2007a).

$$\mathrm{LSTc} = \mathrm{LST} + K_{\mathrm{L}} \times \mathrm{DEM} \quad (5)$$

where LSTc is elevation adjusted LST; LST is the land surface temperature in Kelvin before the correction; DEM is the digital elevation model in meters above sea level, and $K_{\mathrm{L}}$ is the assumed lapse rate of air moving along the terrain. The value 0.0065 K/m is the standard environmental lapse rate correction factor. Adjustment of LST to LSTc is necessary to normalize the LST values associated with the extreme evaporative conditions as air moves over rising or falling terrain. Allen et al. (2007a) described the fitting of unique lapse rates to each image. The enhanced SSEB uses LSTc instead of LST to calculate the ET fractions in Eq. (2). To differentiate the

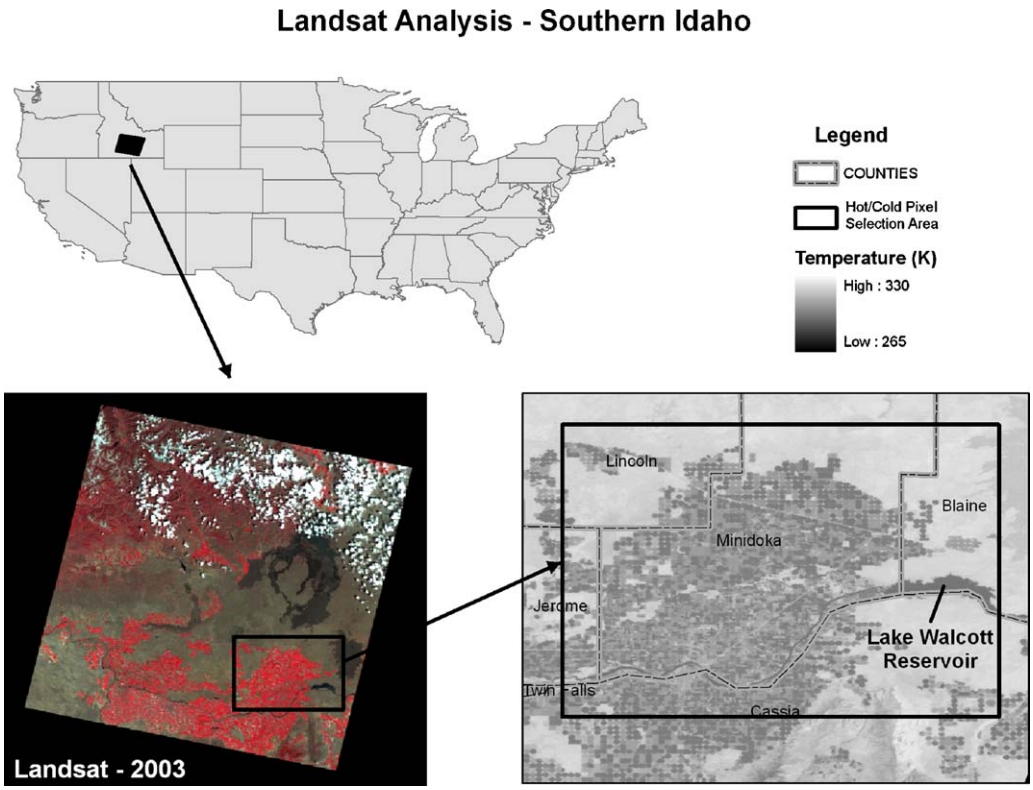


**Fig. 1.** Study site showing a false color composite of 6/28/2003 Landsat image. Hot and cold pixels were selected from within irrigated areas located in southern Minidoka, southeastern Lincoln, eastern Jerome, and northern Cassia counties of southern Idaho. Hot pixels were chosen from within the non-irrigated fields of this study boundary, while cold pixels were systematically picked from high-NDVI center pivot fields.

elevation enhancement from the other corrections that will be discussed later, the elevation corrected model is labeled SSEBel in this manuscript.

### 3.3.2. NDVI correction

The NDVI correction applies a coefficient that varies from 0.65 to 1.0 (or slightly higher), based on the NDVI of the pixel. Tasumi and Allen (2007) reported that green vegetation with full ground cover resulted in a Landsat-based NDVI of 0.7–0.85 while bare soil areas exhibited NDVI less than 0.2 in southern Idaho. The major assumption is that if a pixel has an NDVI equal to or exceeding 0.7, the pixel is considered to be heavily green-vegetated and will transpire at a maximum rate or more compared to a reference crop if water is not limiting and thus the correction coefficient becomes 1.0 or more. However, if the NDVI approaches 0.0, the correction coefficient approaches 0.65 according to Eq. (6). The 0.7 threshold needs to be verified to hold true for other sensors such as MODIS and AVHRR.

$$\mathrm{ETf(elvi)} = \left(0.35 \times \frac{\mathrm{NDVI}}{0.7} + 0.65\right) \times \mathrm{ETf} \quad (6)$$

where ETf(elvi) indicates the ET fraction that is adjusted by both elevation (el) and vegetation index (vi); normally, NDVI is in the range between 0 and about 0.85 where all negative NDVI values have been set to 0.0; ETf is the elevation adjusted ET fraction according to Eqs. (2) and (5). The 0.7 represents an idealized NDVI value of green well-watered vegetation, where the ET fraction is considered to be 1.0.

There is no sound theoretical basis for choosing the range of 0.65–1.0. However, one explanation for a lower ET fraction from less vegetated areas (low NDVI) compared to densely vegetated areas (high NDVI) for a comparable soil moisture is that more of the net radiation conducts into the bare soil as ground heat flux and thus reducing the available energy for ET (Allen, 2010, Pers. Comm.). In cases where NDVI of a pixel is greater than 0.7, it indicates a denser or taller green vegetation canopy than a reference vegetation which can be justified to have somewhat higher ET. For example, a pixel with an NDVI value of 0.8 will increase the ET fraction by 5% to $1.05 \times$ ETf. This procedure is analogous to METRIC's use of a 1.05 multiplier in the determination of the cold pixel ETrF.

To differentiate the inclusion of the NDVI-based correction to the original formulation, the notation of SSEBelvi is used when referring to the ET fraction that is generated by Eq. (6) in this manuscript.

If the NDVI is less than or equal to 0.0, the correction factor will be 0.65, i.e., 35% lower ET than what is estimated by the thermal coefficient alone. NDVI pixels for a land surface are generally above 0.0, especially when NDVI is calculated from top of the atmosphere reflectance values in the near infrared and red bands. In rare situations when a pixel contains mixed features such as water bodies, contamination with clouds, shadows and wet bare soil, the NDVI value could be negative. A water body, whose NDVI is generally negative, will be reset to 0.0 before its use in the SSEB model, and thus a water body will have the maximum correction of 0.65. Coincidently, this correction is close to the approximate correction coefficient that is used to estimate ET of a water body which is between 0.6 and 0.7 as compared to a reference maximum ET (Allen, 2010, Pers. Comm.).

A schematic representation of the SSEB model is shown in Fig. 2. The simplified diagram illustrates how the separation of the 'weather data' (ETo) and remotely sensed data (LST and NDVI) would allow an easy computation to generate ETa in a relatively simple model setup.

Spatially explicit reference ET (ETo) can be produced with the Penman–Monteith equation using net radiation (Rn), temperature ($T$), wind ($U$), relative humidity (RH) and air pressure fields ($P$) either from a point-based weather station or a grid-based model-

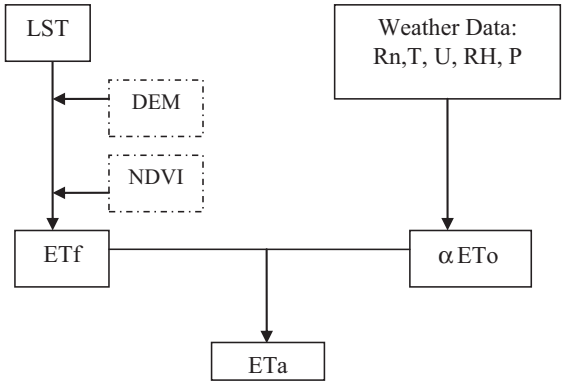


**Fig. 2.** Schematic representation of the SSEB modeling setup. Suggested $\alpha$ is 1.2 when ETo is based on clipped grass reference ET. Rn is net radiation; $T$ is air temperature; $U$ is wind speed; RH is relative humidity; $P$ is atmospheric pressure.

assimilated weather data set. DEM and NDVI are used to correct LST-based ETf for elevation and land cover effects as shown above in Eqs. (5) and (6). Since the magnitude of the ETa is dependent on the accuracy of the ETo, caution should be taken when using model-assimilated gridded weather data sets for ETo estimation since they may not represent reference crop environments. ASCE-EWRI (2005) provides guidance on applying adjustment to GDAS type of data to compensate for the lack of evaporative conditioning.

### 3.4. Analysis procedure

The comparison between SSEB and METRIC models is made both in spatial and temporal space. In this study the METRIC model output is considered as the truth because of its widely distributed use, publications, and the traceability of the Idaho applications to precision weighing lysimeters that were previously located at Kimberly (Allen et al., 2007b).

Spatial comparison is based on a single image dated 6/28/2003. This image represents the middle of the growing season when a mix of vegetation cover can be found, from senescence in winter wheat to mature crops from spring planting. The temporal analysis was conducted using 7-images from the 2003 growing season on 6 arbitrarily selected polygon averages whose location was determined through visual inspection from the June 28 NDVI image to capture different crop-stage or cover types (Fig. 3c). Cloud contaminated pixels (located in the mountainous northern part of the study site) were removed from both METRIC ETrF and SSEB ETf images using an arbitrary threshold value of SSEB ETf > 1.2. NDVI was calculated from the digital numbers (DNs) of the red and near-infrared bands (Goward et al., 1985) from readily available data. This resulted in negative NDVI values in certain bare areas and generally lower values in vegetated surfaces. Although NDVI from DNs and from at-sensor reflectance are linearly related ($r^2 = 0.99$, diagnostic data not presented), there is more relative bias in the low NDVI range (bare ground: about 0.1 when DN NDVI is close to 0.0) than in high NDVI ranges (green vegetation: about 0.8 when DN NDVI is close to 0.74). Since the main effort of this study was to demonstrate the relative impact of using NDVI, as compared to no NDVI, on ET fractions on a given image, all analyses were based on the readily available DN data set. Thus, all negative NDVI values were set to 0.0 before applying the SSEB modeling procedure. Similarly, all negative ETrF and ETf values were also set to 0.0. Negative ETrF and ETf values are generated in pixels where the LST is higher than the chosen HOT-pixel values. These tend to occur in more desert areas, away from an agricultural setting. Seasonal ET was calculated using time-weighted ET fractions (ETf and ETrF) and ETm values, i.e., the average of two consecutive image-date values was multiplied by the number of days in the period to get a period-sum ET. Seasonal sum represents the 144 days between April 9 and August 31, 2003.

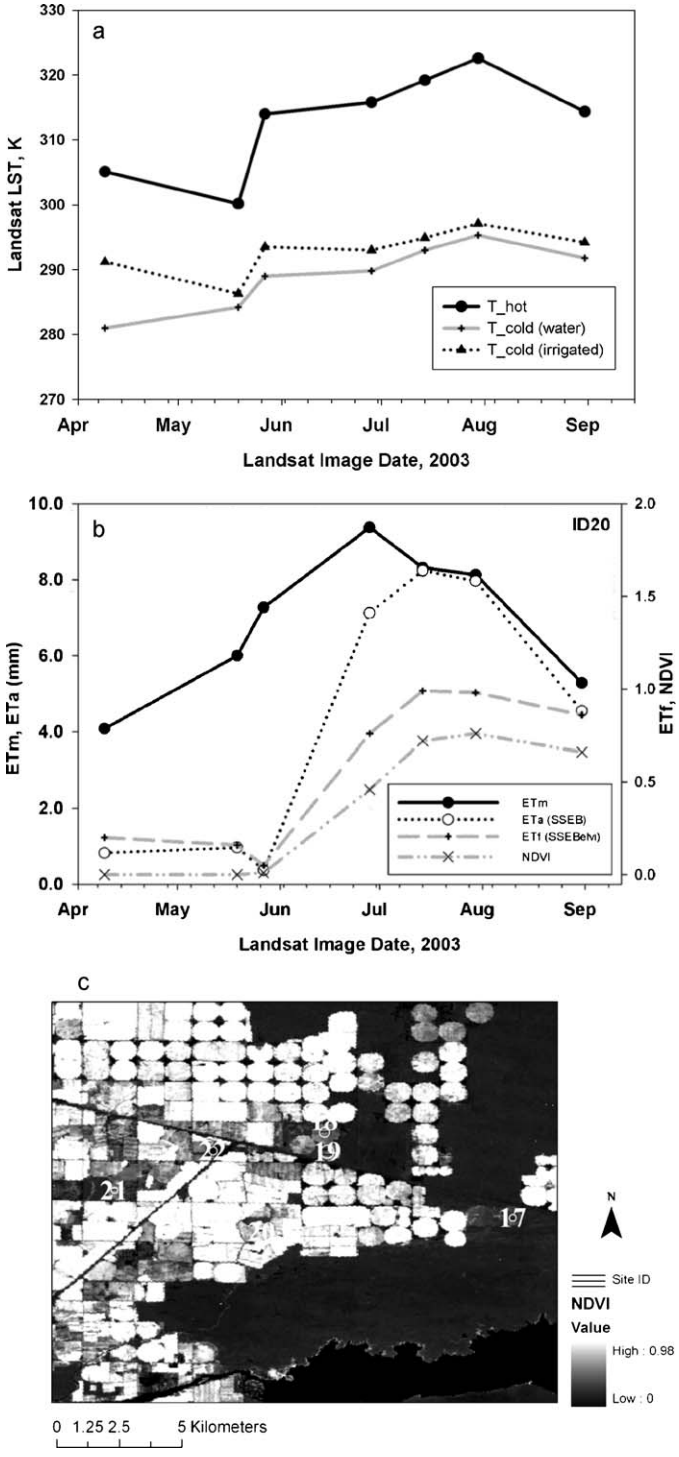


**Fig. 3.** Temporal patterns of the average hot and cold-pixel LST values (a); the relationship between ETm, ETa, ETf and NDVI for site ID20 (b); the location of the sample points is shown on an NDVI image (6/28/2003) (c). The approximate location of this image is shown in Fig. 1. Site IDs 17–22 are used for the temporal analyses shown in Fig. 7a–e.

Scatter plots between SSEB and METRIC were generated using randomly selected 1026 points that represent average values of 1-km by 1 km polygons. Of the 1026 points, 828 were located in areas with elevations under 2000 m while the rest were located

above the 2000 m reference. The 2000 m was used to differentiate the performance of the models between homogeneous and complex terrain. Visual inspection of the Hydro1K elevation data set (Verdin and Jenson, 1996) was used to set this threshold. Basic correlation statistics and graphic scatter plots were used to evaluate the performance of the SSEB model against the METRIC model. Significance of correlation statistics was tested using the correlation *t*-test at 95% confidence interval (Davis, 1973) for individual "*r*" values and using the Fisher's *z*-transformation (Fisher, 1938) for comparing improvements between two correlation statistics.

## 4. Results and discussion

The results of this study are presented in spatial and temporal groups. The graphical relationship between the spatial and temporal analysis is shown in Fig. 3, showing selected sites where temporal comparison was conducted.

Since the introduction of the elevation correction is straightforward, based on established knowledge, comparison with METRIC was not made before and after elevation correction. All comparisons (spatial or temporal) between METRIC and SSEB are thus based on (1) elevation correction alone (SSEBel) and (2) with both elevation and NDVI correction combined (SSEBelvi).

### 4.1. General

The temporal evolution of the average HOT and COLD LST values in the season is shown in Fig. 3a. Generally, pixels with LST values close to the COLD line will have ETf close 1.0 while pixels with LST values close to the HOT line will have ETf close to 0.0. Note that two types of cold-pixel values are shown for comparison purposes. For this study, cold pixels from irrigated fields were used. However, comparison with cold-pixel selected from a water body shows close temporal patterns with a seasonal-peak difference of about 11% (excluding April 9) in relation to the difference between the hot and cold pixels in the study. A notable exception is the disparity on the April 9 image where the cold pixel from an irrigated field was much warmer in relation to the water body, with the difference between the two reaching about 42% of the range between the hot and cold pixels for the same date. The main reason for this was the lack of dense-green vegetation (a low maximum NDVI value of 0.42 at the cold pixel) at the early part of spring that can transpire at the maximum (ETm) rate. Although METRIC addresses this problem by using an NDVI-based correction for calculating ETrF cold (Allen et al., 2007a), this is a weakness in this study. However, this illustrates the benefit of using a water body for future use in SSEB for the cold pixel since SSEB does not use an adjustment factor for establishing ET fraction of the cold pixel during off-peak season when dense vegetation may not be available for selection. The use of a water body for the cold pixel is especially important when working with the 1 km thermal data from MODIS. Allen et al. (2007a) pointed out the difficulty of locating MODIS land pixels that meet the maximum ET fraction requirement.

The relationships between ETf, NDVI, ETm and ETa using a representative data point from an irrigation field (ID20) are demonstrated in Fig. 3b. The temporal patterns of ETf and ETa are influenced by the temporal patterns of both ETm and NDVI. Thus, both ETf and ETa tend to peak during the time between the peak periods of ETm and NDVI. Because ETm is heavily influenced by net radiation and temperature, the peak ETm occurred on June 28 when compared to the other 6 image dates. ETa peaked on July 14, while the NDVI peaked on July 30 (Fig. 3b, Table 2). This pattern appears to hold for all other sample locations (Fig. 7a–e) in that NDVI peaks occur later than ETf. The significance of this observation highlights the fact that ETa is both a function of the available energy (ETm) and the land cover condition (NDVI) as affected by the growth stage and availability of water. Therefore, the timing of the peak ETa may not necessarily coincide with the peak timing of neither ETm nor NDVI.

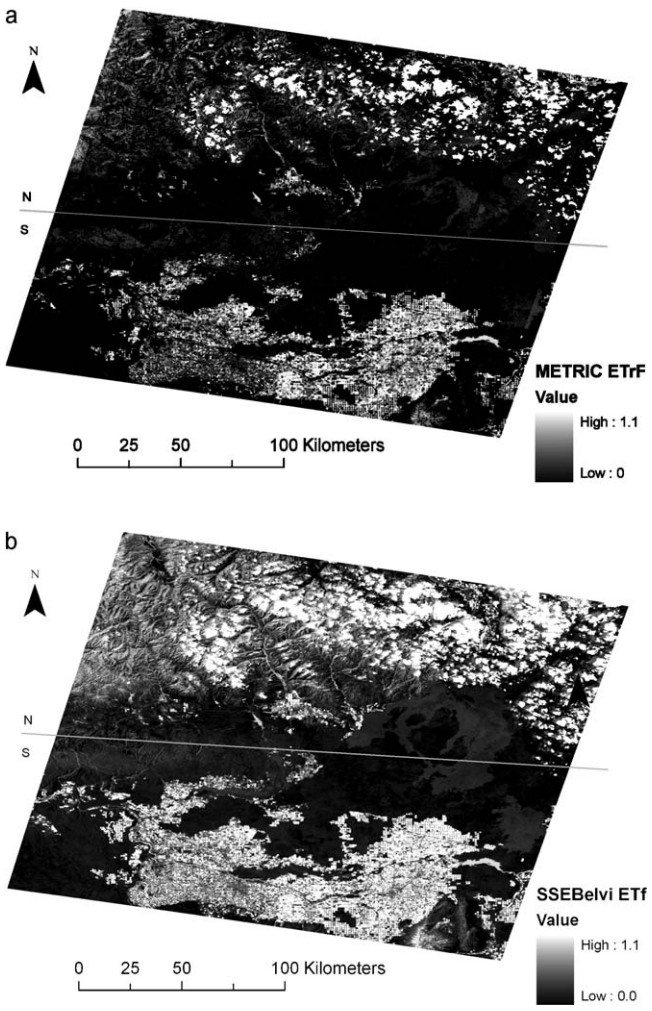


**Fig. 4.** ET fraction: METRIC (a) and SSEBelvi (b), June 28, 2003. Generally, brighter areas represent well vegetated, irrigated fields with high ET fractions. But bright areas in northern part of the image are due to "no data" values from cloud contamination.

### 4.2. Spatial

ET fraction maps from both METRIC and SSEBelvi models for 6/28/2003 imagery are shown in Fig. 4a and b. The general spatial patterns of ETf (SSEBelvi) and ETrF (METRIC) are comparable, especially in the southern part of the image where the topography is more uniform and dominated by irrigated fields. However, there is some inconsistency in the magnitude and pattern of ET fractions from both models on the mountainous part of the image, with complex topography predominantly located in the northern half of the image (Fig. 4a and b). The straight line shown in the figures roughly divides the northern higher elevation and complex topography areas from the southern irrigated fields that have homogeneous topography.

The effect of the NDVI correction on the performance of the two SSEB model versions (SSEBelvi vs. SSEBel) in relation to METRIC is shown on two elevation groups (Fig. 5a–d). The NDVI effect on less complex topography is shown in Fig. 5a and b while more complex topography is shown in Fig. 5c and d. The inclusion of the

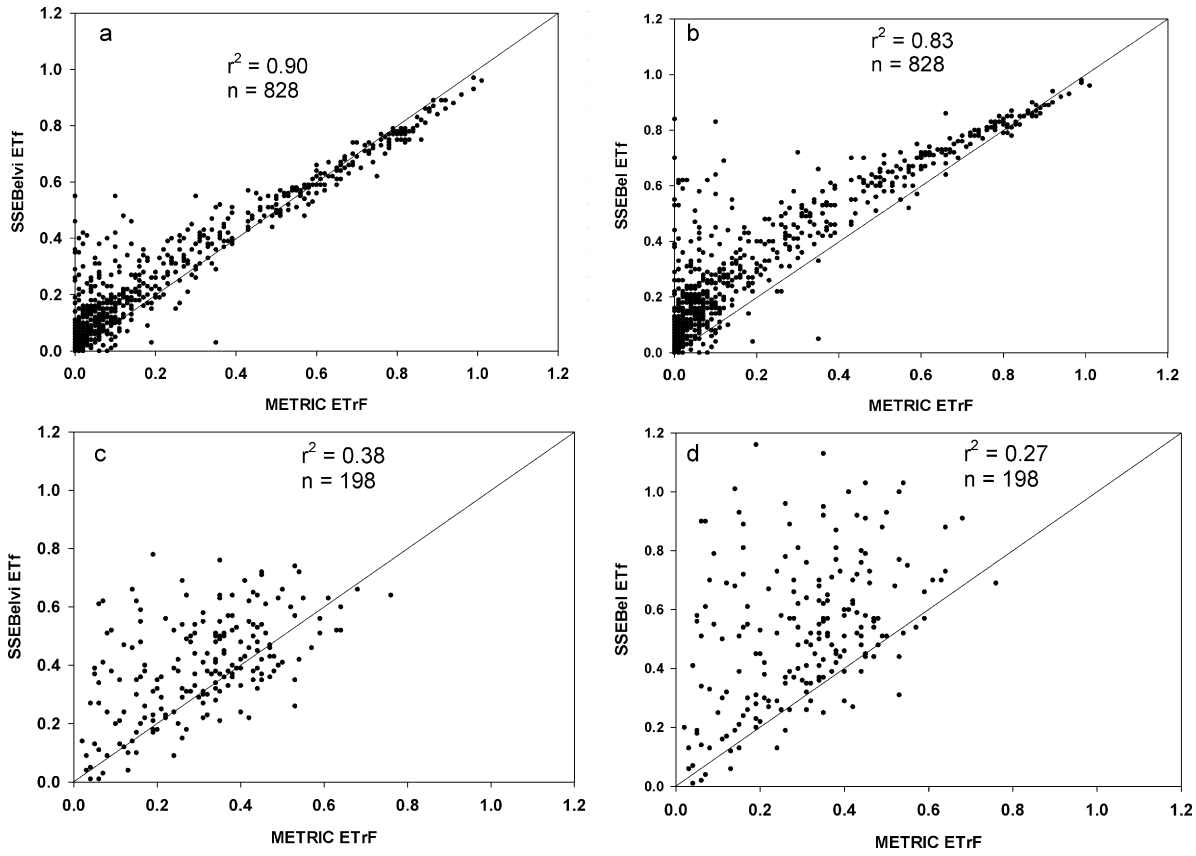


**Fig. 5.** Scatter plots between SSEB and METRIC ET fractions: "a" and "b" for elevation less than 2000 m: (a) SSEBelvi vs. METRIC; (b) SSEBel vs. METRIC; "c" and "d" for elevation greater than 2000 m: (c) SSEBelvi vs. METRIC; (d) SSEBel vs. METRIC.

NDVI correction coefficient in SSEBelvi has a statistically significant improvement (using Fisher's *z*-transformation test) over the standard elevation correction in SSEBel where the correlation coefficient "*r*" has increased from 0.91 to 0.95 using samples in the "under 2000 m elevation" group (Table 3, Fig. 5a and b). The NDVI correction improved the scatter in the lower ET fraction regions as well as the slope of the relationship in relation to the 1:1 line. Without the NDVI correction (Fig. 5b), two slopes can be identified, a steeper (with an overestimation) at lower than 0.5 ET fraction and a less steep (close to the 1:1 line) at higher than 0.5 ET fractions. On the other hand, Fig. 5a shows a tighter scatter with an improvement in the slope, close to the 1:1 line. We can still see a slight overestimation in the lower ETf ranges (ETf < 0.4) and a slight underestimation in the higher end (ETf > 0.8). The higher end under estimation can be related to the fact that SSEBelvi does not use the 1.05 multiplier for the cold ETf.

The improvement in the correlation (*r*) between METRIC and the two SSEB versions is even greater on the higher elevation group with elevation greater or equal to 2000 m. The "*r*" increased significantly from 0.52 to 0.62 (Table 4) when SSEBelvi is compared instead of SSEBel. Despite the correlation improvement in a relative sense, the relationship between SSEB and METRIC was weaker for the higher elevation samples compared to the lower elevation group.

In order to understand the potential causes of the poor performance of SSEB in higher elevation areas in relation to METRIC, the independent relationship between NDVI and ET fractions from both METRIC and SSEB was evaluated. This is based on the presence of a well-established strong relationship between NDVI and ETa. Tables 3 and 4 show how NDVI is correlated strongly with both METRIC and SSEB in the "lower" elevation group and poorly in higher elevations. The correlation between NDVI and METRIC ETrF ($r = 0.91$) and with SSEBelvi ETf (0.88) is comparable (Table 3) for the lower areas. On the other hand, for the mountainous areas, NDVI was poorly correlated with both METRIC ($r = 0.4$) and SSEBelvi ($r = 0.13$). Although both SSEB and METRIC correlated poorly

**Table 3**
Correlation matrix among METRIC ETrF, SSEB ETfs, NDVI and DEM for elevation less than 2000, $n = 828$.

| | DEM | NDVI | METRIC | SSEBel | SSEBelvi |
|---|---|---|---|---|---|
| DEM | 1.00 | | | | |
| NDVI | −0.09 | 1.00 | | | |
| METRIC | −0.27 | 0.91 | 1.00 | | |
| SSEBel | −0.16 | 0.82 | 0.91[a] | 1.00 | |
| SSEBelvi | −0.19 | 0.88 | 0.95[a] | 0.99 | 1.00 |

*Note*: all "*r*" values are significant at 95% ($\alpha = 0.05$) confidence level.

[a] The improvement in correlation between METRIC and (SSEBel or SSEBelvi) is significant with Fisher's *z*-transformation statistics at 95% ($\alpha = 0.05$). Others were not tested.

**Table 4**
Correlation matrix among METRIC ETrF, SSEB ETfs, NDVI and DEM for elevation 2000 and above, $n = 198$.

| | DEM | NDVI | METRIC | SSEBel | SSEBelvi |
|---|---|---|---|---|---|
| DEM | 1.00 | | | | |
| NDVI | −0.40 | 1.00 | | | |
| METRIC | −0.07* | 0.44 | 1.00 | | |
| SSEBel | 0.08* | −0.10* | 0.52[a] | 1.00 | |
| SSEBelvi | −0.03* | 0.13 | 0.62[a] | 0.97 | 1.00 |

[a] The significant improvement in correlation as in Table 3. Others were not tested for improvement.

* Correlation is not significant at 95% ($\alpha = 0.05$) confidence level. The rest are all significant.

with NDVI in complex terrain, it suggests that SSEB has more difficulty than METRIC in representing ET processes in higher elevations and/or complex topography. This may be due to the fact that SSEB does not take into account slope and aspect in calculating the net radiation while the "mountain-model" of METRIC used in this study accounts for the slope and aspect when calculating the net radiation.

The scatter plots in Fig. 5a and b (elevation less than 2000 m) show that not only the correlation, but also the magnitude of the METRIC ETrF and SSEB ETf is comparable. The slight underestimation of SSEB on the higher end (values close to 1.0) can be explained by the fact that METRIC ETrF includes a 1.05 multiplying coefficient to give a 5% increase for a well vegetated crop, compared to a reference surface. However, the impact of the factor can be partially offset by the NDVI correction procedure where pixels with NDVI > 0.7 will have ETf more than 1.0. On the other hand, if the user chooses the water body which was about 11% cooler (Fig. 3a) there will be a general underestimation by the model. Therefore, users should account for differences in the choice of the reference cold pixels and their relation with LST of a well vegetated surface.

The overestimation of SSEB with respect to METRIC on the lower end was reduced by the use of the NDVI correction in SSEBelvi (Fig. 5a) compared to SSEBel (Fig. 5b). Further examination of the location of the overestimated values in the lower end (METRIC ETrF < 0.2) showed that most of these pixels are located (result not presented) in the complex topographic region (top, right of Landsat image, Fig. 1) with elevations higher than 1500 m. Similarly, Fig. 5c and d shows that the use of SSEBelvi has improved the relationship between METRIC and SSEB both in magnitude and slope in relation to the 1:1 line, despite the overall all poor performance of the SSEB model in the complex topographic region. The advantage of SSEBelvi over SSEBel seems more pronounced in the complex topography. Other factors that can influence the relationship with METRIC are the differences in the selection of both the HOT pixel (lower end) and COLD pixel (higher end). Since the two models (METRIC and SSEB) used different hot and cold pixels, it is difficult to conclude whether the overestimation is systematic.

The importance of using the NDVI to correct the ET fraction is illustrated further in Fig. 6a–c. When SSEB does not use the NDVI to correct the ETf, a general overestimation of the ETf is shown at low NDVI values. Using the concept of "warm" and "cold" edges in the NDVI–Ts plot (trapezoid method of Moran et al., 1996) or (triangle method of Carlson, 2007) where the Ts or (Ts – Ta) is replaced by ETf in this case, arbitrary lines are drawn to demonstrate the concept. For a given NDVI value, pixels close to the cold edge will have higher ET (less moisture stress) than pixels close to the warm edge (more stressed vegetation). Thus, without the NDVI correction as shown in Fig. 6a, high ET fractions (close to cold edges) can be observed especially when NDVI is lower than 0.3. The fact that most of the scatter is located in topographically complex regions, the main explanation for this could be that some of the data points (low NDVI, high ETf) could be coming from northern slopes (with shadows) and contamination with clouds that tend to reduce the NDVI but make the LST cooler; thus, increase ETf. Furthermore, it is possible that a lack of parameterization for albedo and soil heat flux for a mix of land cover (bare soil, senescing and green vegetation) may contribute to the scatter in the lower NDVI ranges. Although we are not providing a physical explanation on the use of the NDVI correction, we also think that the NDVI correction may be accounting for the non-linearity in the relationship between sensible heat and LST that the SSEB model is not considering unlike the METRIC model.

The improvement in correlation between METRIC and SSEB is shown in Fig. 6b and c, where SSEBelvi ETf and METRIC ETrF are compared in terms of their relationship with NDVI. In both cases (SSEBelvi and METRIC) pixels have moved from the cold to the warm edge when compared to SSEBel (Fig. 5a). The movement is highest at low NDVI values. This demonstrates that the incorporation of NDVI correction is more important in low NDVI cover areas. On the other hand, if the vegetation cover is uniform and with an NDVI value ≥0.4, the correction from NDVI may not be necessary. The NDVI threshold value of 0.4 has also been used by Nemani and Running (1995) to classify cover types into 4 different groups in an NDVI–Ts space.

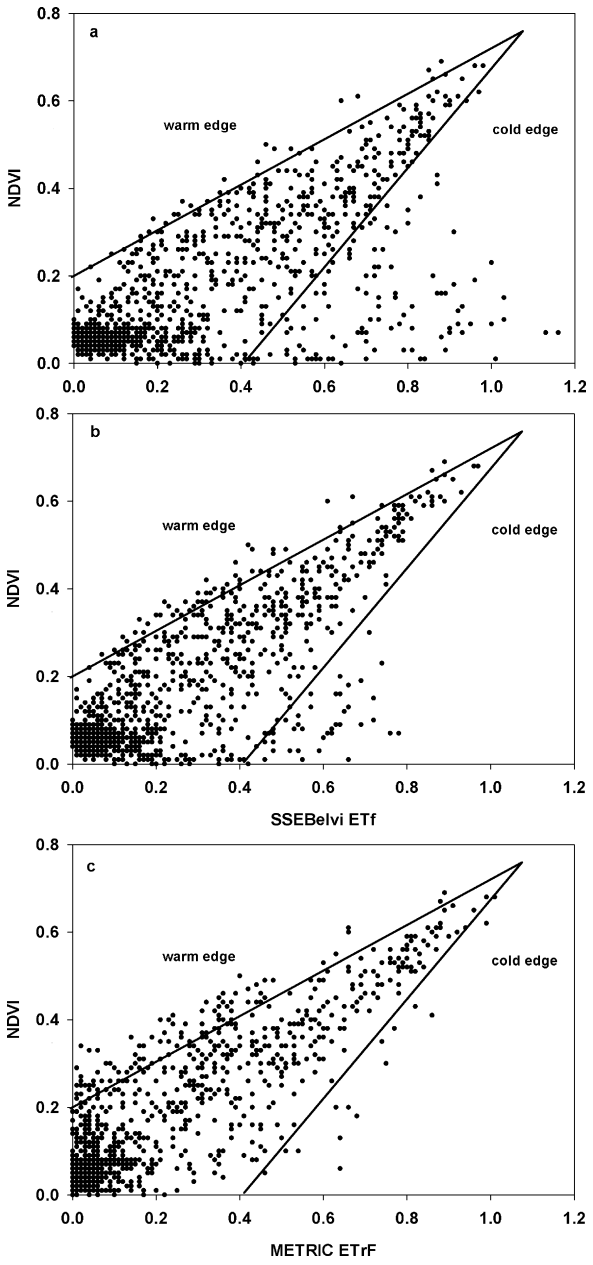


**Fig. 6.** Scatter plots between NDVI and different ET fractions: NDVI against (a) SSEBel, (b) SSEBelvi, (c) METRIC. Cold and warm-edge lines are drawn arbitrarily for comparison purposes. Total number of data points is 1026, pooled from high and low elevation groups.

### 4.3. Temporal

The temporal patterns of METRIC ETrF and two SSEB ETf versions (SSEBel and SSEBelvi) and the corresponding NDVI for 6 arbitrarily selected locations in the southeastern part of the study site are shown in Fig. 7a–e. Because the reference maximum ET (ETm) for

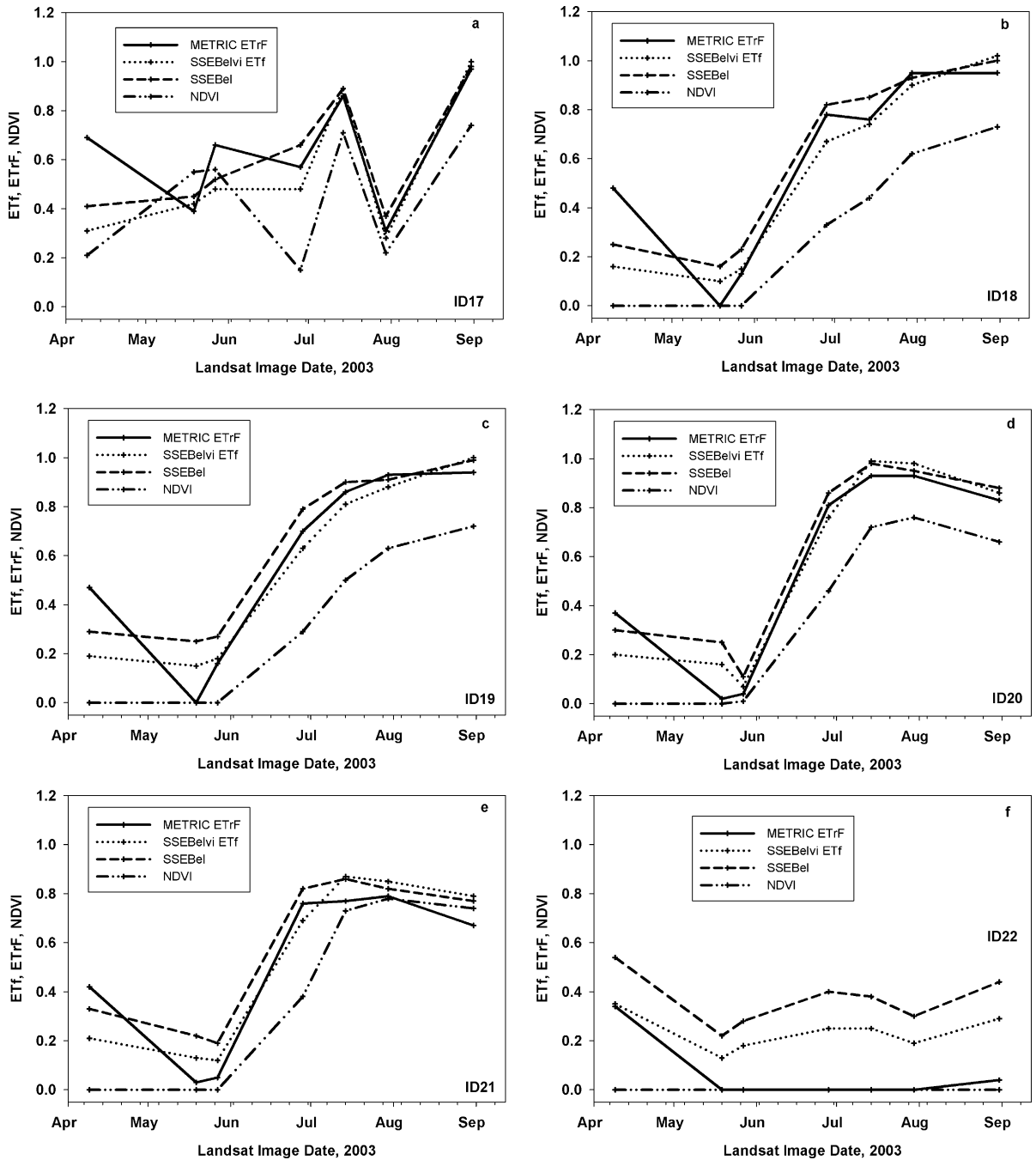


**Fig. 7.** Temporal plots of three ET fractions and NDVI for: (a) ID17; (b) ID18; (c) ID19; (d) ID20; (e) ID21; and (f) ID22. Location of IDs is shown in Fig. 3c. NDVI = 0.0 is a result of using digital numbers instead of reflectance values for NDVI calculations.

these location is effectively identical (due to proximity of the locations), ETa was not shown in these charts for clarity as it will have the same temporal pattern as the ET fraction of the corresponding models.

Site ID17 appears to be an alfalfa field with cyclical cutting and growing periods where the NDVI peaks and troughs alternated at least 2 times during the growing season from April through August (Fig. 7a). Generally, both METRIC and SSEB ET fractions showed similar alternating patterns during the season. Similarly the magnitudes of the ET fractions between METRIC and SSEB (both versions) are comparable. The notable exception is the relatively higher METRIC ETrF (0.7) on April 9, compared to 0.3 or 0.4 for SSEB versions. The higher difference in the early season has also shown up in all sites except site ID22 (Fig. 7e).

Site IDs 18 and 19 show comparable temporal patterns in all model ET fractions and NDVI (Fig. 7b and c). This may be due to physical proximity of two sites (Fig. 3c) which may be subject to similar cropping and irrigation regimes. On both cases, the lowest NDVI was observed on May 21 and the peak on the August 31 image. Both SSEBel and SSEBelvi corresponded well in pattern and magnitude with METRIC during the time period between May 27 and August 31, with SSEBelvi being slightly lower than METRIC and SSEBel being higher than METRIC. The notable difference is the high value of METRIC on April 9 and its lowest value (0.0) on May 19. Further investigation of the April 9 comparison revealed that the METRIC process has assigned a non-zero ETrF for the HOT pixel due to recent rainfall while SSEB assigned an ETf of 0.0 for the April 9 HOT-pixel (1st data point) shown in Fig. 3a. However, the HOT pix-

els for the two models are not the same so direct comparison of the ET fraction is difficult. On the other hand, the choice of the COLD pixel can also have an impact on the ET fraction, especially on the early season when a dense vegetation may not be available. As an example, early in the growing season a cold pixel from a vegetation field tends to be warmer (42%) compared to a cold pixel from a water body, thus potentially increasing the ET fraction of most pixels (Fig. 3a).

The major discrepancies between METRIC and SSEB appeared during the early part of the season when both ETm and NDVI are low, which will amount to a lower maximum ETa estimate. Thus, the early season differences will have a lesser impact on seasonal total ET and water balance estimation when using either of the models.

Site IDs 20 and 21 also show comparable patterns with low (before May 27) and peak (July 30) NDVI occurring at about the same time period (Fig. 7d and e). The corresponding ET fractions occurred on an earlier date (July 14). Note that for the study region that includes the six study sites, the peak ETm occurred even earlier on June 28 (Fig. 3b). This consistency shows the usefulness of understanding the relationship between ETm, ETa and NDVI for water management purposes. On both Fig. 7d and e, SSEBelvi ETf is more than both SSEBel ETf and METRIC ETrF, when the NDVI values are more than 0.70. This of course is according to the formulation of the NDVI-based correction where NDVI = 0.70 is considered to be a reference NDVI value that represents full canopy cover and healthy vegetation that provides ETa at the maximum ET rate when there is no water limitation.

A summary for site ID20 of the daily and seasonal total comparison between METRIC and SSEB model parameters is presented in Table 2. When both models were subject to the same ETm, the seasonal ETa estimate between METRIC and SSEBelvi produced a difference of only 17 mm (2.8%), i.e., seasonal SSEB ETa was 613 mm while that of METRIC was 596 mm with a seasonal total ETm of 1008 mm. This illustrates the potential of SSEB in estimating peak and seasonal ETa accurately, in relation to METRIC, despite the apparent disparity between the two models during the early season when ETa is generally low.

Site ID22 represents a field devoid of vegetation with NDVI of 0.0 or less throughout the season (Fig. 7f). Image analysis of the field shows that it is located at the intersection of two major roads with potential urban structures (roads, parking lots and open fields). Both models showed low ET fractions with METRIC showing 0.0 for much of the season. On the other hand, SSEBel appeared to overestimate by about 50% more than that of SSEBelvi. Although the SSEBelvi ETf is not very high and may be justified during periods within rainfall events over bare ground, the consistent value of around 0.20 throughout the season when METRIC showed 0.0 needs to be investigated.

Both the spatial and temporal comparisons of METRIC and SSEB indicate that the LST-based scaling for ET is promising in providing comparable results to a more complex energy balance model in space and time.

The additional enhancements introduced for SSEB with respect to topography is consistent with the lapse-rate correction recommended by METRIC. The NDVI correction in SSEB has increased the correlation with METRIC in low NDVI regions (NDVI < 0.4), especially areas found in more complex topographic region of south central Idaho. The NDVI correction can be an optional procedure to be recommended in estimating ET in diverse vegetation and topographic regions, with minimal gain on irrigated fields located in flat topography with similar agro-hydrologic settings.

Although more research is required to understand the exact relationship between land cover mixture and ET, a comparison with the METRIC model seems to suggest this simple formulation can be used to help account for land cover mixture differences that result in differences in albedo and ground heat flux transfer compared to a clipped reference grass environment.

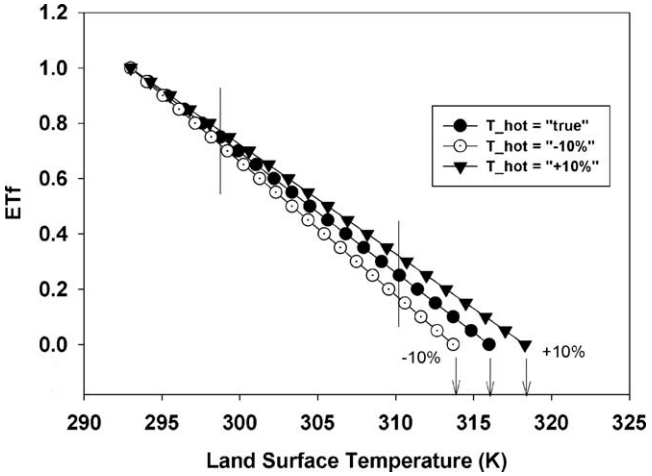


**Fig. 8.** Sensitivity of ETf to changes in the selection of the hot pixel. A 10% over- or under-estimation of the hot pixel will result in about 30% error for ETf = 0.25, but only 3% error for ETf = 0.75.

Although both METRIC and SSEB provided comparable results with independent set of HOT and COLD pixels in this study, the choice of the hot and cold pixels can influence the ET rate. As shown in Fig. 3a, the cold pixel selection can bring a marked difference (42%) whether the selection is made from a water-body or a green-vegetation site. This is generally a problem in the early part of the season when dense green vegetation cannot be found. Allen et al. (2007a) have outlined procedures in making sure both the HOT and COLD reference pixels represent their supposed minimum and maximum ET fraction rates, respectively.

From our experience, it is generally easier to select the correct cold pixel (ETf = 1.0) than the correct hot (ETf = 0.0) pixel. Assuming the cold pixel is selected correctly, from basic linear scaling, an error in the selection of the hot pixel would result in a much higher error in the lower ETf ranges than in the higher ETf pixels. For example, when the difference between the hot and cold is 23 K (June 28 image), a 10% error (2.3 K) in the hot pixel value will result in an error of about 30% or higher for ETf of 0.25 or less, but only an error of about 3% or lower for ETf of 0.75 or higher as illustrated in Fig. 8.

If a user does not have the expertise or time to ascertain the reliability of HOT and COLD pixel values for large scale operational applications, we recommend consistency in the location of the extreme pixels. For the cold pixel, we recommend the identification of a water body whose LST varies temporally with the green vegetation (example: avoid snowmelt fed water bodies) for much of the season and always pick the cold pixel from it at the different part of the season. Similarly, for the hot pixel, identify an area (extent would vary for MODIS and Landsat) where there is a good chance of finding hot pixels in much of the season, and pick the hot pixels from this area to avoid selection of hot pixels from a different hydro-climatic zone. This procedure ensures precision because the month-to-month and year-to-year seasonal ET values are comparable, but the absolute accuracy of the ET can be biased depending on the representativeness of the extreme pixels. Consistent seasonal ET values are useful for estimating relative crop performance and drought. However, hydrologic water balance estimation requires accurate ET magnitudes. This creates a great opportunity to integrate the SSEB approach and the METRIC process to satisfy the need to processing large amounts of remotely sensed data quickly at a reasonable cost (SSEB), but with validation and potential parame-

terization to be provided by the more robust and accurate METRIC process on selected new sites.

## 5. Conclusions

The comparison between METRIC and SSEB demonstrated that there is a positive and strong relationship between METRIC and SSEB justifying the use of SSEB for large scale monitoring. The fact that the SSEB model compared well with METRIC in a region with elevation ranges between 800 m and 2000 m (low elevation group) suggests the incorporation of a lapse-rate correction to the LST is reasonable.

The study also demonstrated that the inclusion of an NDVI-based correction in SSEBelvi has improved the performance of the model with respect to METRIC, especially on low NDVI regions. This complements the weak performance of existing VI-based ET models in accounting for the contribution of wet soil surfaces (low NDVI) to the total ET flux. Similarly, the poor parameterization of albedo, ground-heat flux and radiation balance in complex topography also created a weaker relationship between the SSEB thermal index alone (SSEBel) and METRIC ETrF in low NDVI ranges. Thus, the combination of the thermal index and its enhancement with NDVI in SSEBelvi appear to address the weaknesses of both VI-based and thermal-based indices for actual ET estimation in agricultural and naturally vegetated regions where the variability in albedo is not extreme. The method does not account for land surface temperature changes that are caused by extreme albedo differences found in desert and snow covered environments.

Thus, both an elevation correction and land cover correction will provide an enhanced performance of the SSEB model in vegetated regions. Both corrections are relatively easy to incorporate to the original formulation of the SSEB that was designed to be applied in uniform topography with irrigation basins in mind. However, the NDVI correction was more useful on sparsely vegetated areas with low NDVI values such as early crop conditions and mountainous regions where poor parameterization of the ground heat flux and slope/aspect factors can influence the ET estimation. We also recommend the use of NDVI that is based on reflectance data instead of digital numbers to avoid its underestimation.

The study also found that both the SSEB and METRIC ET fractions showed weaker correlation with NDVI in complex terrains, suggesting the difficulty of the existing methods in estimating actual ET in complex terrains. Possible improvement in the SSEB model may include the inclusion of a slope-aspect correction to handle the effect of solar-shadows in the energy balance equation.

In this study, the timing of the peak for ETm, ETa and NDVI occurred in this order, reinforcing the common knowledge in the dependence of actual ET (ETa) both on energy supply (ETm) and vegetation condition (NDVI).

We believe that SSEB has captured both the spatial and temporal variability of the METRIC model reasonably well. SSEB has a potential for large scale agro-hydrologic applications to estimate actual ET with inputs of LST, NDVI, DEM, and reference ET in most agricultural settings where complex topography is not a dominant feature.

## Acknowledgements

Funding was provided through the USGS/EROS support for the Geographic Science Center of Excellence (GIScCE), South Dakota State University. We acknowledge the use of METRIC-based data sets made available by Dr. Richard Allen and his research team at the University of Idaho. We also thank Dr. Allen for a variety of suggestions made during comparisons between SSEB and METRIC and during preparation of this manuscript. We are also grateful to Dr. Susan Moran for her important comments and suggestions. We thank our colleagues at EROS, Lei Ji, Guleid Artan and Mike Crane for their valuable technical comments and edits.

## References

Allen, R.G., 2010. Personal communication with Dr. Richard Allen, an expert in the field.
Allen, R.G., Pereira, L., Raes, D., Smith, M., 1998. Crop Evapotranspiration. Food and Agricultural Organization, Rome.
Allen, R.G., Pruitt, W.O., Wright, J.L., Howell, T.A., Ventura, F., Snyder, R., Itenfisu, D., Steduto, P., Berengena, J., Yrisarry, J.B., Smith, M., Pereira, L.S., Raes, D., Perrier, A., Alves, I., Walter, I., Elliott, R., 2006. A recommendation on standardized surface resistance for hourly calculation of reference ETo by the FAO56 Penman–Monteith method. Agric. Water Manage. 81, 1–22.
Allen, R.G., Tasumi, M., Morse, A.T., Trezza, R., 2005. A Landsat-based Energy Balance and Evapotranspiration Model in Western US Water Rights Regulation and Planning. J. Irrig. Drain. Eng. 19, 251–268.
Allen, R.G., Tasumi, M., Morse, A.T., Trezza, R., Kramber, W., Lorite, I., Robison, C.W., 2007a. Satellite-based energy balance for mapping evapotranspiration with internalized calibration (METRIC) – applications. ASCE J. Irrig. Drain. Eng. 133, 395–406.
Allen, R.G., Tasumi, M., Trezza, R., 2007b. Satellite-based energy balance for mapping evapotranspiration with internalized calibration (METRIC) – model. ASCE J. Irrig. Drain. Eng. 133, 380–394.
Allen, R.G., Tasumi, T., Torres, I.L., 2004. Investigations and Refinements to the METRIC Satellite Image Processing Procedure for More Accurate Prediction of Evapotranspiration from Desert and Cities. University of Idaho, p. 20.
Anderson, M.C., Norman, J.M., Diak, G.R., Kustas, W.P., Mecikalski, J.R., 1997. A two-source time-integrated model for estimating surface fluxes using thermal infrared remote sensing. Remote Sens. Environ. 60, 195–216.
Anderson, M.C., Norman, J.M., Mecikalski, J.R., Otkin, J.A., Kustas, W.P., 2007. A climatological study of evapotranspiration and moisture stress across the continental United States based on thermal remote sensing: 1. Model formulation. J. Geophys. Res. 112, doi:10.1029/2006JD007506.
ASCE-EWRI, 2005. In: Committe, A.E.S.o.R.E.T. (Ed.), The ASCE Standardized Reference Evapotranspiration Equation. ASCE Reston, Reston.
Bastiaanssen, W.G.M., Menenti, M., Feddes, R.A., Holtslag, A.A.M., 1998. A remote sensing surface energy balance algorithm for land (SEBAL): 1. Formulation. J. Hydrol. 198–212, 212–213.
Bastiaanssen, W.G.M., Noordman, E.J.M., Pelgrum, H., Davids, G., Thoreson, B.P., Allen, R.G., 2005. SEBAL model with remotely sensed data to improve water-resources management under actual field conditions. J. Irrig. Drain. Eng. 131, 85–93.
Carlson, T., 2007. An overview of the "triangle method" for estimating surface energy evapotranspiration and soil moisture from Satellite imagery. Sensors, 1612–1629.
Choudhry, B.J., 1991. Multispectral satellite data in the context of land surface heat balance. Rev. Geophys. 29, 217–236.
Davis, J.C., 1973. Statistics and Data Analysis in Geology. John Wiley and Sons, New York.
Dexter, R., 1999. Diurnal and seasonal albedo trends of wheat at the Bratt's lake observatory, Saskatchewan. M.Sc. Thesis. Department of Geography, Simon Fraser University.
Fisher, R.A., 1938. Statistical Methods for Research Workers. Oliver and Boyd, Edinburgh.
Florinsky, I.V., Kulagina, T.B., Meshalkina, J.L., 1994. Influence of topography on landscape radiation temperature distribution. Int. J. Remote Sens. 15, 3147–3153.
Goward, S.N., Cruickshanks, G.D., Hope, A.S., 1985. Observed relation between thermal emission and reflected spectral radiance of a complex vegetated landscape. Remote Sens. Environ. 18, 137–146.
Goward, S.N., Waring, R.H., Dye, D.G., Yang, J., 1994. Ecological remote sensing at OTTER: satellite macroscale observations. Ecol. Appl. 4, 322–343.
Gowda, P.H., Chavez, J.L., Colaizzi, P.D., Evett, S.R., Howell, T.A., Tolk, J.A., 2008. ET mapping for agricultural water management: present status and challenges. Irrig. Sci. 26, 223–237.
Gowda, P.H., Senay, G.B., Howell, T.A., Marek, T.H., 2009. Lysimetric evaluation of Simplified Surface Energy Balance approach in the Texas high plains. Appl. Eng. Agric. 25, 665–669.
Jackson, R.D., Idso, D.B., Reginato, R.J., Pinter Jr., P.J., 1981. Canopy temperature as a crop water stress indicator. Water Resour. Res. 17, 1133–1138.
Kalma, J.D., McVicar, T.R., McCabe, M.F., 2008. Estimating land surface evaporation: a review of methods using remotely sensed surface temperature data. Surv. Geophys. 29, 421–469.
Kustas, W.P., Norman, J.M., 2000. A two-source energy balance approach using directional radiometric temperature observations for sparse canopy covered surfaces. Agron. J. 92, 847–854.
Markham, B.L., Barker, J.L., 1986. Landsat MSS and TM post-calibration dynamic ranges, exoatmospheric reflectances and at-satellite temperatures. EOSAT Landsat Tech. Notes 1, 3–7.
Menenti, M., Choudhury, B.J., 1993. Parameterization of land surface evaporation by means of location dependant potential evaporation and surface temperature range. Exchange processes at the land surface for a range of space and time scales. In: Proceedings of the Yokohama Symposium.

Moran, M.S., Clarke, T.R., Inoue, Y., Vidal, A., 1994. Estimating crop water deficit using the relation between surface-air temperature and spectral vegetation index. Remote Sens. Environ. 49, 246–263.
Moran, M.S., Jackson, R.D., Raymond, L.H., Gay, L.W., Slater, P.N., 1989. Mapping surface energy balance components by combining Landsat Thematic Mapper and ground-based meteorological data. Remote Sens. Environ. 30, 77–87.
Moran, M.S., Rahman, A.F., Washburne, J.C., Goodrich, D.C., Weltz, M.A., Kustas, W.P., 1996. Combining the Penman–Monteith equation with measurements of surface temperature and reflectance to estimate evaporation rates of semiarid grassland. Agric. For. Meteorol. 80, 87–109.
Nemani, R., Pierce, L.L., Running, S.W., Goward, S.N., 1993. Developing satellite derived estimates of surface moisture status. J. Appl. Meteorol. 32, 548–557.
Nemani, R., Running, S.W., 1995. Satellite monitoring of global land cover changes and their impact on climate. Clim. Change 31, 395–413.
Nemani, R., Running, S.W., 1989. Testing a theoretical climate-soil-leaf area hydrologic equilibrium of forests using satellite data and ecosystem simulation. Agric. For. Meteorol. 44, 245–260.
Price, J.C., 1989. Using the spatial context, in satellite data to infer regional scale evapotranspiration. IEEE Trans. Geosci. Remote Sens. 28, 940–948.
Roerink, G.J., Su, Z., Menenti, M., 2000. S-SEBI: a simple remote sensing algorithm to estimate the surface energy balance. Phys. Chem. Earth 25, 147–157.
Senay, G.B., Budde, M.E., Verdin, J.P., Melesse, A.M., 2007. A coupled remote sensing and Simplified Surface Energy Balance approach to estimate actual evapotranspiration from irrigated fields. Sensors 7, 979–1000.
Senay, G.B., Verdin, J.P., Lietzow, R., Melesse, A.M., 2008. Global daily reference evapotranspiration modeling and evaluation. J. Am. Water Resour. Assoc. 44, 969–979.
Su, Z., 2002. The Surface Energy Balance System (SEBS) for estimation of turbulent heat fluxes. Hydrol. Earth Syst. Sci. 6, 85–99.
Su, Z., Mccabe, M.F., Wood, E.F., 2005. Modeling evapotranspiration during SMACEX: comparing two approaches for local- and regional-scale prediction. J. Hydrometeorol. 6, 910–922.
Tasumi, M., Allen, R.G., 2007. Satellite-based ET mapping to assess variation in ET with timing of crop development. Agric. Water Manage. 88, 54–62.
Tasumi, M., Trezza, R., Allen, R.G., Wright, J.L., 2005. Operational aspects of satellite-based energy balance models for irrigated crops in the semi-arid U.S. J. Irrig. Drain. Sys. 19, 355–376.
Verdin, K.L., Jenson, S.K., 1996. Development of continental scale DEMs and extraction of hydrographic features. In: Third International Conference/Workshop on Integrating GIS and Environmental Modeling, Santa Fe, New Mexico.
Warner, T.A., Chen, X., 2001. Normalization of Landsat thermal imagery for the effects of solar heating and topography. Int. J. Remote Sens. 22, 773–788.